Journal of Petrology Advance Access published December 4, 2015

JOURNAL OF PETROLOGY

Journal of Petrology, 2015, 1–20
doi: 10.1093/petrology/egv060
Original Manuscript

OXFORD

The Role of Viscous Particle Segregation in Forming Chromite Layers from Slumped Crystal Slurries: Insights from Analogue Experiments

Mélanie Forien[1]*, Jonathan Tremblay[1], Sarah-Jane Barnes[1], Alain Burgisser[2,3] and Philippe Pagé[1]

[1]Sciences de la Terre, Université du Quebec à Chicoutimi, 555 Boulevard de l'Université, Chicoutimi, QC G7H 2B1, Canada; [2]CNRS, ISTerre, 73376 Le Bourget du Lac, France; [3]Université Savoie Mont Blanc, ISTerre, 73376 Le Bourget du Lac, France

*Corresponding author. Present address: Department of Geology, University of Tromsø, Dramsveien 201, 9037 Tromsø, Norway. E-mail: melanie.forien@uit.no

Received July 30, 2014; Accepted September 9, 2015

ABSTRACT

The question of how the mineral layering in layered intrusions forms has been extensively debated for many decades. There are many types of layering and it is of course possible that a number of mechanisms are involved. Of particular interest is how chromite layers form, because these may contain valuable metals (such as platinum-group elements) in addition to Cr. One model for the formation of these layers is that they formed through slumping of semi-consolidated cumulates from the margins of the intrusion into the magma chamber. During this slumping, the grains are sorted by density and/or size differences. This study examines the viability of this process using analogue modelling. Starting materials (beads and glycerine) were scaled to match the density and size of the minerals (chromite, orthopyroxene and plagioclase) present in layered mafic–ultramafic layered intrusions and to match the density and viscosity of the silicate magma. A Perspex flume tank divided by a removable partition at one end was fully filled with glycerine. A homogenized mixture of the beads was placed in the smaller partition of the tank (representing the margins of the magma chamber). The tank was then inclined between 16° and 45°. The partition was removed and the beads flowed into the main part of the box. The experiments were recorded by video camera, allowing us to follow the dynamics of the flow during each run. Segregation of the beads was observed in the final deposits: the larger, less dense beads (representing plagioclase) concentrated at the top of the flow, with the intermediate-sized and medium density beads (representing orthopyroxene) in the middle and the smaller, denser beads (representing chromite) at the bottom, thus mimicking natural examples. In experiments where the angle of inclination was low, long, thin layers formed, such as those found in the Bushveld Complex. In experiments where the angle of inclination was high, thick but short layers formed. A dimensionless analysis allows better understanding of the dynamics of the flow. At the macroscopic scale, the flow regime is strongly influenced by the viscosity of the fluid and is considered macro-viscous, where the role of the interstitial liquid is non-negligible.

Key words: cumulate formation; experimental modelling; viscous particle segregation; layering; slumping slurries

INTRODUCTION

The mineralogical layering in layered intrusions may reflect differences in texture, mineralogy or the modal proportion of minerals in the rocks (Irvine, 1982). Of particular interest are chromite-rich layers. Many of these contain high concentrations of economically important metals, including Cr and the platinum-group elements (PGE), and consequently such deposits have been extensively studied. A classic example of layering involving chromite layers in a layered intrusion is the chromite layers of Upper Group 1 (UG1) of the Bushveld Complex, South Africa, at Dwars River, which consist of an alternation of chromitite and anorthosite (Fig. 1a). Chromite layers are also observed in the ultramafic Monchegorsk pluton, Kola peninsula, Russia (Fig. 1b) and at the centimetre scale (Fig. 1c) or micro scale (Fig. 1d) in the Stillwater Igneous Complex. However, despite the well-known occurrences of these massive centimetre- to metre-scale layers, which can extend for kilometres in single intrusions, their origin and evolution remain highly debated.

Various cumulate-forming processes have been proposed, including the following: mixing of a primitive magma with a felsic magma (Irvine, 1975; Kinnaird *et al.*, 2002; Nex, 2004; Kottke-Levin *et al.*, 2009) or with a more evolved resident magma (Irvine, 1977; Eales, 1987; Naldrett *et al.*, 2009, 2012); layers with double diffusion convection (McBirney & Noyes, 1979; Huppert & Sparks, 1984; Wilson *et al.*, 1987); oxygen fugacity fluctuations (Cameron & Desborough, 1964; Ulmer, 1969; Cameron, 1975; Murck & Campbell, 1986); pressure variations (Cameron, 1980; Lipin, 1993; Cawthorn, 2005); crystallization in a staging magma chamber then injection of the crystal slurry into the final repository

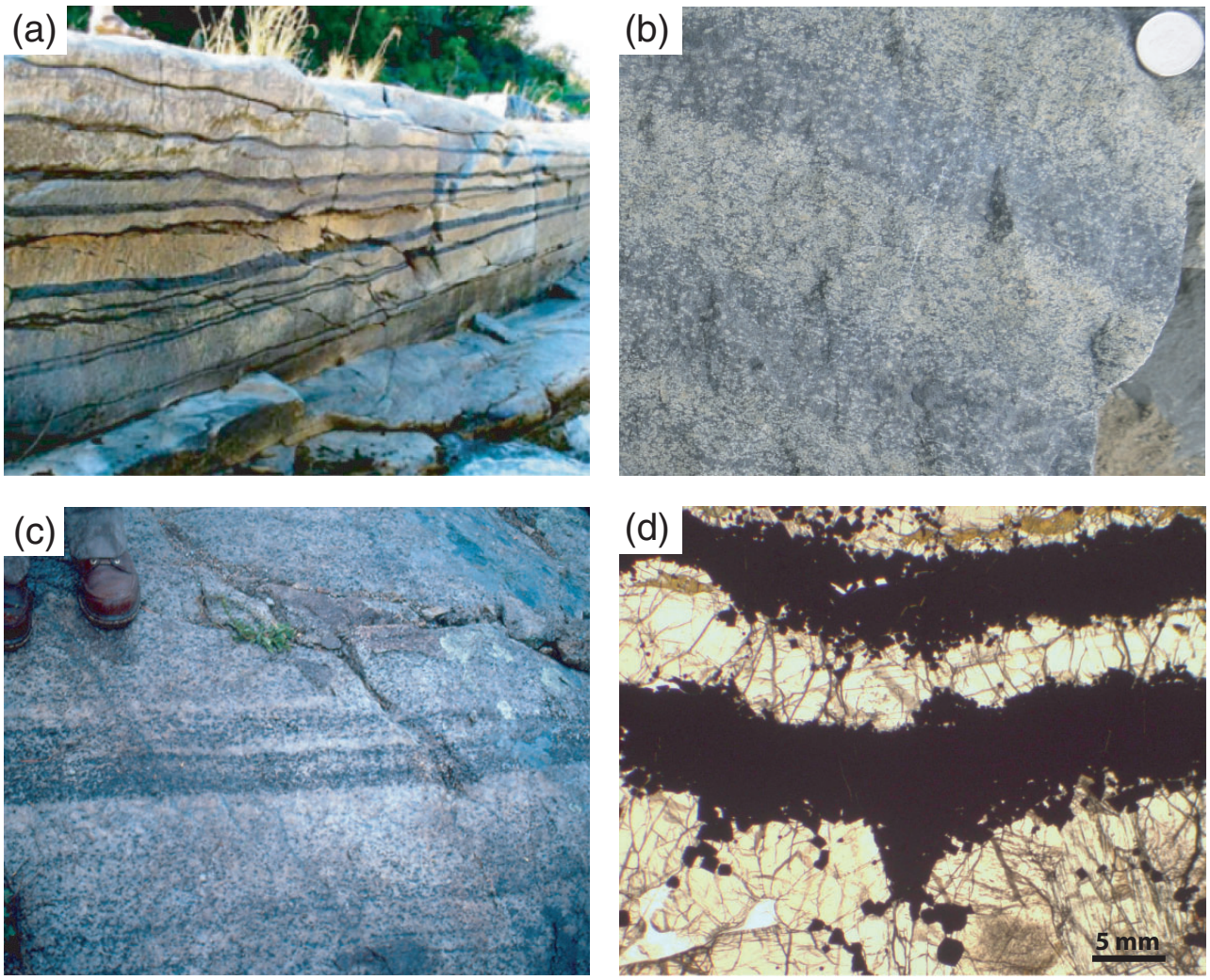

Fig. 1. Field photographs and photomicrograph of chromitite layers from layered intrusions. (a) Chromitite seams exposed at Dwars River in the Bushveld Igneous Complex (South Africa). (b) Chromitite layers in the Sopcheozero deposit in the ultramafic rocks of the Monchegorsk pluton, Kola Peninsula (Russia). Chromitite layers within pyroxenite. (c) Chromite-bearing layers hosted in gabbronorite at Mountain View in the Stillwater Complex (Montana, USA). (d) Photomicrograph of alternating chromite layers in the Stillwater Complex (Montana, USA). Photographs (a), (c) and (d) taken by Sarah-Jane Barnes.

(Eales, 2000; Marsh, 2007; Mondal & Mathez, 2007; Voordouw *et al.*, 2009); and slumping of semi-consolidated cumulates (Maier *et al.*, 2013). Reviews of some of these processes have been provided by Naslund & McBirney (1996) and Naldrett *et al.* (2012).

In this study, we evaluate the hypothesis of Maier *et al.* (2013) that the slumping of semi-consolidated cumulates located on the side-wall of a magma chamber could result in the layering observed in some intrusions. Flows of dense particles have been studied previously (Hodson, 1998; Blanchette *et al.*, 2004) and much of the basic physics has been verified using laboratory experiments (Bonnecaze *et al.*, 1993; Simpson, 1999; Huppert, 2006). The most widely used configuration for these is dam-break experiments. This configuration involves release of a mass of particles inside a channel by the removal of a vertical barrier. These dam-break experiments have been used to study the dynamics of Newtonian fluids on a slope (Huppert, 1982), and to determine the rheology of suspensions in a viscous liquid (Castruccio *et al.*, 2010) and the rheology of floods and pyroclastic density currents (Balmforth *et al.*, 2007; Roche *et al.*, 2008). Here, we use the evolution of dam-break flows to observe the segregation of a mix of particles with different sizes and densities suspended in a viscous fluid, using scaling parameters to match an unconsolidated mafic cumulate containing a small amount of chromite. After describing the experimental procedure, we then describe the processes occurring during the flow and the structure of the final deposits. Limitations of the analogue experiments are also be discussed. Finally, the results are compared with natural examples, showing that our experiments result in the formation of layers similar to those observed in layered intrusions.

EXPERIMENTS

Starting material and apparatus

It is important to scale the densities and viscosities of the experimental materials to those of the natural minerals and silicate melt. The scaling procedure is based on standard similarity conditions, as developed by Hubbert (1937), Ramberg (1981) and Barenblatt (2003). In this study we conducted small-scale experiments with a mixture of different ball flows in a dam-break set-up. The focus lies on the spatial distribution of particles and liquid in the flow.

The flow is mainly governed by the following set of physical parameters (Hutter, 1984): g, *U*, *H*, *d*, ρ and ν, where *g* is the gravity acceleration, *U* is the downslope velocity, *H* is depth, *d* is the particle diameter, ρ is the density of the particles and ν is the kinematic viscosity of the fluid ($= \mu/\rho$, where μ is the absolute or dynamic viscosity).

In this study, special care was taken with regard to the parameter ρ^* (ρ_{exp}/ρ_{nature}), which represents the ratio between ρ_{exp}, the density of the analogue materials used in the experiments, and ρ_{nature}, the density of their natural equivalent. In the experiments the particles were scaled as closely as possible to crystals in a mafic magma chamber. Silicone ($\rho_{l(exp)} = 1300\,kg\,m^{-3}$), polyacetal ($\rho_{m(exp)} = 1410\,kg\,m^{-3}$) and glass beads ($\rho_{s(exp)} = 2520\,kg\,m^{-3}$) were selected to simulate plagioclase ($\rho_{l(nature)} = 2700\,kg\,m^{-3}$), pyroxene ($\rho_{m(nature)} = 3100\,kg\,m^{-3}$) and chromite ($\rho_{s(nature)} = 4790\,kg\,m^{-3}$) crystals, respectively. In this way, the density ratio ρ^*(silicone/plagioclase) was *c.* 0·48, ρ^*(polyacetal/pyroxene) was 0·45 and ρ^*(glass/chromite) was 0·53. Glycerine ($\rho_f = 1260\,kg\,m^{-3}$; $\mu = 1{\cdot}41\,Pa\,s$) was used to represent the silicate liquid with a density $\rho_{silicate\ liquid} = 2640\,kg\,m^{-3}$ and a viscosity $\mu_{silicate\ liquid} = 2{\cdot}82\,Pa\,s$. The density ratio between glycerine and its natural equivalent, ρ^*(glycerine/silicate liquid), was 0·48. All these materials were chosen so as to keep the densities and, in the case of the liquid, the viscosity, in the same ratios to the natural materials, with an overall scaling ratio of ~0·5 (Table 1).

The choice of the diameters of the beads was constrained in large part by the choice of densities and by what is commercially available. The densest beads (the proposed chromite analogue) were the smallest (1 mm) and the lightest (plagioclase analogue) were the largest (4·3 mm). The exact sizes of the natural grains in the

Table 1: Physical properties and ratios of experimental over natural values (scaling factors)

Parameter and dimension	Analogue of	Symbol	Typical values		
			Model	Natural equivalent	Scaling factor
Particle diameter (m)					
Glass beads	Chromite	d_s	$1{\cdot}0 \times 10^{-3}$	$5{\cdot}0 \times 10^{-4}$–$2{\cdot}0 \times 10^{-3}$	0·50–2·00
Polyacetal balls	Pyroxene	d_m	$2{\cdot}0 \times 10^{-3}$	1×10^{-3}–2×10^{-3}	1–2
Silicone balls	Plagioclase	d_l	$4{\cdot}3 \times 10^{-3}$	1×10^{-3}–5×10^{3}	1–4
Particle density (kg m^{-3})					
Glass beads	Chromite	ρ_s	2520	4790	0·53
Polyacetal balls	Pyroxene	ρ_m	1410	3100	0·45
Silicone balls	Plagioclase	ρ_l	1300	2700	0·48
Fluid density (kg m^{-3})	Silicate melt	ρ_f	1260	2640*	0·48
Fluid viscosity (Pa s)	Silicate melt	μ	1·41	2·826*	0·50
Gravity acceleration (m s^{-2})	—	g	9·81	9·81	1
Slope (degree)	—	α	16–45	5–35	1·28–3·20

*Based on PELE estimation for the B-1 magma of Bushveld at 1115°C and 3 kbar with 1·0 wt % water. Composition from Barnes *et al.* (2010). Global value range for natural silicate melt densities is between 2500 and 3000 kg m^{-3} (McMillan *et al.*, 1989; Sparks *et al.*, 1993), and for natural melt viscosities is between 1 and 10^9 Pa s (McMillan *et al.*, 1989; Shaw, 1972).

marginal zone of an intrusion at the time of slumping are not known but, assuming that they are slightly greater than those of the chill and slightly smaller than the size of the grains in the cumulate part of the intrusion, the scaling factor for the grain size would be around unity (Table 1). Also, owing to the combined requirement for consistency in the beads—that is, the beads of one type had all to be exactly the same—and the constraints on the density and size differences of the three types of bead, only spherical beads were available. Thus, the grain size ratio of the experimental particles and natural crystals $d^*(d_{exp}/d_{nature})$ was unity, corresponding to the grain size of the natural case.

The beads were different colours (red for chromite, white for pyroxene and black for plagioclase), whereas the liquid and the flume tank were transparent, allowing a clear view of the behaviour of the beads during the flow.

The experimental apparatus (Fig. 2a and b) comprised a Perspex tank, 102 cm long, 15 cm wide and 30 cm high. This was fixed to a support, inclinable up to 45° from the horizontal by two threaded bars located on each side of the box. A sliding gate was positioned 15 cm from one end (Fig. 2b). Unfortunately, it would have been very difficult to construct a tank scaled to the dimensions of a natural magma chamber, so the length scale was applicable only during the flow, as the box did not represent the length-to-width ratio of a magma chamber.

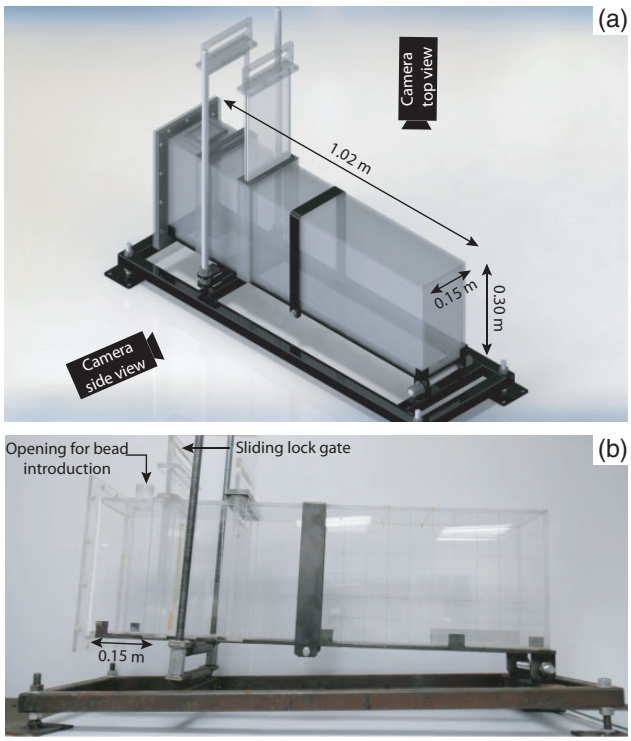

Fig. 2. Digital image (a) and photograph (b) of the Perspex flume tank used for the experiments. A sliding gate separates the 'reservoir' from the rest of the tank. The beads are homogeneously distributed in the reservoir until the sliding gate is removed. Two camera recorders, placed on the top and on the side of the box, were used to film the flow and the formation of the deposit.

EXPERIMENTAL PROCEDURES

Two main series of experiments with different proportions of glass beads (the chromite analogue) were carried out: (1) seven experiments were conducted using 5 vol. % of silicone, 5 vol. % of polyacetal and 0·5 vol. % of glass beads; (2) four experiments were conducted using 5 vol. % of silicone, 5 vol. % of polyacetal and 10 vol. % of glass beads (Table 2). The second series allowed better visualization of the glass bead deposits in the tank.

The tank was completely filled with glycerine, the gate was installed, and then the small compartment (the analogue for the marginal zone of the intrusion) was emptied of glycerine. The bead mixture was introduced into the small compartment. It proved challenging to keep the bead mixture homogeneous as it was placed in the small compartment. To produce a homogeneous mixture, all of the polyacetal and silicone beads and one-third of the glass beads were mixed and placed in the compartment. Then, the remaining two-thirds of the glass beads were added so that they percolated through the already present beads to form an overall homogeneous dry mixture.

Glycerine was then slowly added to the small compartment in a quantity such that the particle proportions were respected, which corresponds to 89·5 vol. % for series 1 and 80 vol. % for series 2. One end of the Perspex tank was then elevated until the desired angle was attained. After ensuring that the initial beads bed was still and settled, the experiment started when the mixture was released by rapidly lifting the sluice gate. During run-out the kinematics of the flow and deposition were measured by two video cameras: one giving the top view and the other the side view (Fig. 2a). An inclined mirror placed underneath the tank allowed the side video camera to capture a bottom view (Fig. 2a) of what was happening at the base of the flow. After complete stabilization of the balls in the tank, the final deposits were photographed. We systematically measured the mean velocity U_f of the flow for each inclination angle α. The transparency of the base of the tank allowed measurement of the mean velocity of the glass beads layer, U_s (the chromite analogue), located at the flow base (Table 2).

One additional experiment was carried out to investigate whether it was possible to model the cyclic behaviour of some chromite layers. For this case, the total volume of the beads was divided into three. After the first run-out, the gate was replaced into the initial position, and then a second batch of beads was introduced into the starting compartment and released. This process was repeated after the second slumping. This experiment was carried out with a slope of 17·26°.

Table 2: Run conditions and results

Run	α (deg)	Red beads (vol. %)*	White balls (vol. %)*	Black balls (vol. %)*	U_l (m s^{-1})	U_s (m s^{-1})	U_f (m s^{-1})	Grain-flow thickness (m)	Reynolds number	Froude number	Shear rate (m s^{-1})	Bagnold number	Savage number	Friction number
MB016	30·8	0·5	5	5	2·56E – 4	2·00E – 4	2·28E – 4	1·53E – 2	1·67E – 4	1·32E – 3	1·49E – 2	1·02E – 3	7·17E – 9	1·26E + 5
MB017	40·8	0·5	5	5	1·22E – 3	5·59E – 4	8·89E – 4	1·38E – 2	6·52E – 4	5·49E – 3	6·46E – 2	4·41E – 3	1·34E – 7	2·90E + 4
MB018	36·3	0·5	5	5	6·49E – 4	2·78E – 4	4·64E – 4	1·26E – 2	3·40E – 4	2·78E – 3	3·68E – 2	2·51E – 3	4·32E – 8	5·10E + 4
MB019	27·5	0·5	5	5	1·77E – 4	1·24E – 4	1·50E – 4	1·68E – 2	1·10E – 4	8·56E – 4	8·93E – 3	6·10E – 4	2·58E – 9	2·10E + 5
MB020	20·9	0·5	5	5	3·52E – 5	4·39E – 5	3·95E – 5	1·80E – 2	2·90E – 5	2·20E – 4	2·20E – 3	1·50E – 4	1·57E – 10	8·54E + 5
MB021	17·5	0·5	5	5	1·03E – 5	1·26E – 5	1·14E – 5	1·95E – 2	8·36E – 6	6·28E – 5	5·87E – 4	4·01E – 5	1·13E – 11	3·20E + 6
MB022	45·2	0·5	5	5	2·44E – 3	1·27E – 3	1·85E – 3	1·21E – 2	1·36E – 3	1·19E – 2	1·53E – 1	1·04E – 2	7·42E – 7	1·23E + 4
MB023	30·6	10·0	5	5	3·23E – 3	6·02E – 3	4·62E – 3	1·74E – 2	7·23E – 3	9·60E – 3	2·65E – 1	2·48E – 2	3·12E – 6	9·71E + 3
MB024	20·2	10·0	5	5	9·26E – 4	1·81E – 3	1·37E – 3	2·08E – 2	2·14E – 3	2·73E – 3	6·58E – 2	6·16E – 3	1·95E – 7	3·91E + 4
MB025	25·3	10·0	5	5	2·17E – 3	3·46E – 3	2·82E – 3	2·31E – 2	4·41E – 3	5·72E – 3	1·22E – 1	1·14E – 2	6·72E – 7	2·11E + 4
MB026	16·4	10·0	5	5	2·36E – 4	4·84E – 4	3·60E – 4	1·99E – 2	5·63E – 4	7·09E – 4	1·81E – 2	1·70E – 3	1·47E – 8	1·42E + 5

*Percentage by volume (vol. %) for all the particles referring to the ratio between the volume of the sub-chamber before the gate was lifted and the volume taken up by the particles. U_l is the average velocity of the black balls. U_s is the average velocity of the red beads. U_f is the average velocity of the flow.

RESULTS

Videos

In the Supplementary Data (available for downloading at http://www.petrology.oxfordjournals.org) we provide three videos of the experiments: one of each series (0·5 vol. % and 10 vol. % of red glass beads) and one of the multi-injection experiment. The video recordings were taken from the side view. The first one corresponds to the experiment MB020 in which the starting material was 0·5 vol. % of red glass beads and the tank had an inclination of 20·9°. On the mirror located under the tank, the red glass beads are visible at the base of the flow. In the second video recording, corresponding to the experiment MB024 containing 10 vol. % of red glass beads in the starting materials and with an inclination angle of 20·23°, the mirror reflects only red glass beads because of their major proportion in the starting materials. The third video recording is a montage of the multi-injection experiment. The tank was tilted to 17·55°. The video shows the three flows after the three 'injections' of materials.

Dynamics

The motion of particles is initiated when the inclination of the slope is above a critical angle of repose (θ_c). Many studies have been conducted recently on the loss of stability of a dry granular slope above this critical angle (GDR MiDi, 2004); a few studies have been carried out on underwater slopes (Allen, 1970; Carrigy, 1970; Courrech du Pont *et al.*, 2003) and none on immersion in a viscous liquid such as glycerine. In our study, no flow was observed for experiments with a slope of less than 15°: particles collapsed after the sluice gate was removed and reached only their angles of repose (Fig. 3). In this case, the run-out distance depended only on the inclination angle and the initial column height, as described by Farin *et al.* (2014). These experiments were not included in this study and will not be discussed further.

The mean flow velocity was calculated from an average of measurements taken from the top view at different times of the flow. The measurement was taken over a distance of 10 cm in the last third of the tank, where the flow seemed to reach a constant velocity. The mean flow velocity (U_f) for each experiment is shown in Table 2. Both series of experiments are plotted versus the slope angle in Fig. 4a. This shows that the velocity of the flow increased with an increase in the percentage of smaller particles and with an increase in the slope. In the first series (with 0·5 vol. % of smaller particles), the velocity increased exponentially with increasing slope, whereas the increase with the slope was linear for the second series (with 10 vol. % of smaller particles).

Fig. 3. Experiment with a slope less than 15°. No movement was observed after 1 h.

The velocity of larger black balls, U_l (representing plagioclase with a density $\rho_l = 1300\,\text{kg m}^{-3}$), on the top of the flow and the smaller red beads, U_s (representing chromite with a density $\rho_s = 2520\,\text{kg m}^{-3}$), located at the base of the flow were measured via the video camera located above the tank and the mirror placed under the tank, respectively. The velocities for the two series were measured in the centre of the flow, where the flow velocity was not influenced by the walls of the tank; the data are plotted in Fig. 4b. For the first series (0·5 vol. % red beads), the velocity of the smaller red beads was slower than that of the larger black balls (Table 2). The velocity ratio between the larger and smaller particles was determined graphically and was *c.* 0·49 (Fig. 4b). Thus, we discerned a centre-line velocity gradient developed in the flow itself from the base to the top. However, for the second series of experiments (10 vol. % red beads), the red bead velocity was higher than that of the larger black balls (Table 2). The ratio between the velocities of larger and smaller particles for the second series was approximately 1·79 (Fig. 4b). Furthermore, the proportion of glass beads at the base of the flow influenced the velocity gradient in the flow itself. The velocity of the flow with 10 vol. % small beads was twice that of the flow with 0·5% small beads. Moreover, during slumping, relatively few particles were in true suspension in the fluid because most of them roll or slide onto each other at the bottom of the tank, interacting by collisions.

Characterization of the flow

To characterize the experimental flow regime, the flow Reynolds number Re (the ratio between inertial and viscous forces) was calculated for each experiment (Table 2). The relationship of inertial to viscous force is described by

$$\text{Re} = \rho_M U_f h / \mu_M \quad (1)$$

where ρ_M is the mixture density, U_f is the mean flow velocity, h is the grain flow thickness and μ_M is the viscosity of the grain flow. Assuming a common value of the volumetric concentration in a polydisperse mixture, $\upsilon_s = 0{\cdot}6$, the mixture densities for the first and second series experiments were respectively ~1350 and ~1670 kg m^{-3}. The mixture viscosity, μ_M, is approximately $\mu(1 - \upsilon_s/\upsilon^*)^{-2{\cdot}5}$, where $\upsilon^* = 0{\cdot}74$ is the maximum volume fraction of a closely packed structure of spherical particles (e.g. Choux & Druitt, 2002). The grain flow thickness reported in Table 2 was measured during

the flow around the middle of the box, approximately where the grain flow thickness was uniform. The median value of Re found for both series was 6×10^{-4}. It is well below the limit for a turbulent regime (500–2000) and characterizes a laminar flow. The particle Reynolds numbers, $\rho_f(U_s - U_f)d/\mu$, are between 10^{-3} and 10^{-2}, also well into the laminar regime.

The source Froude number Fr is the ratio of inertial stresses over gravitational stresses:

$$\mathrm{Fr} = U_f \left[\frac{(\rho_M - \rho_f) g \cos\alpha H}{\rho_f}\right]^{-1/2} \quad (2)$$

where g is the gravitational acceleration, α is the inclination angle and H is the bed height before the sluice gate opens (4·92 and 8·50 cm for series 1 and 2, respectively). The median value of Fr for both series is 3×10^{-3}. Such a low value characterizes subcritical flows, the overall propagation speed of which is affected by source dynamics (i.e. the dynamics of the initial bed collapse in our experiments).

The dynamics of the flow can be also described by three other dimensionless numbers that characterize the kinetic processes at play in the flows: the Bagnold number (N_{Bag}), the Savage number (N_{Sav}) and the friction number (N_{Fric}) (Iverson & Vallance, 2001; Bursik *et al.*, 2005). The Bagnold number characterizes the relative importance of the interstitial fluid to the transport of momentum and can be defined as the ratio of grain-collision stress to fluid viscous shear stresses in a granular mixture (Iverson & Vallance, 2001):

$$N_{Bag} = \frac{\rho_s d^2 \gamma}{\mu} \lambda^{1/2} \quad (3)$$

where ρ_s is the solid grain mass density, d is the grain diameter, γ is the shear rate and μ is the dynamic viscosity of the fluid. In our experiments, the shear rate was estimated by dividing the observed flow speeds by the flow thicknesses, as reported in Table 2. The value λ corresponds to the linear concentration of spherical grains related to the volumetric concentration υ_s by

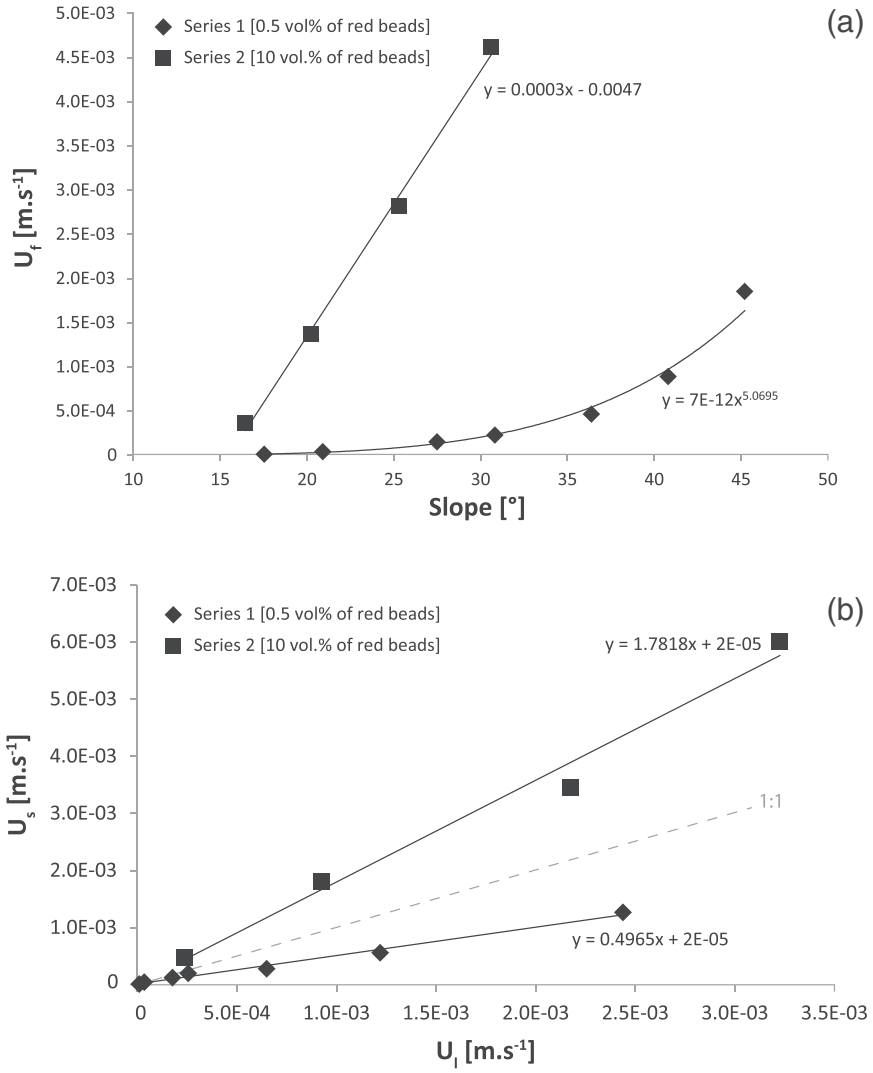

Fig. 4. (a) Velocity profiles for Series 1 and 2 experiments showing the mean velocity of the flow (U_f) versus the slope for each experiment. (b) Velocity profiles for Series 1 and 2 showing the velocity of the red glass beads (U_s) versus the velocity of the black silicone balls (U_l). Data are given in Table 2.

$\lambda = \upsilon_s^{1/3}/(\upsilon_*^{1/3} - \upsilon_s^{1/3})$, where υ_* is the maximum possible grain concentration. Values for the Bagnold number were approximately 3×10^{-3} for the first series and 10^{-2} for the second series. These values indicate that the collisional stresses were much lower than the viscous stresses. Hence, the material is said to be in the macro-viscous regime ($N_{Bag} \leq 40$), in which the interstitial fluid plays a significant role in momentum transfer, such as for flows of slurries or debris flows (Iverson, 1997).

The Savage number is defined as the ratio of collisional over frictional solid stresses (Iverson, 1997):

$$N_{Sav} = \frac{\rho_s d^2 \gamma^2}{(\rho_s - \rho_f) g h} \quad (4)$$

where h is the depth below the flow surface. This dimensionless number accounts for the relative significance of enduring contact friction and collisions among particles. If N_{Sav} is larger than 0·1, the grain inertial stress dominates the contact friction stress in granular flows. Otherwise, a small N_{Sav} indicates that collisions probably transmit little stress in such flows and contact friction must dominate (Savage & Hutter, 1989). Values of N_{Sav} in our experiments were approximately 10^{-7} for series 1 and 10^{-6} for series 2, which indicates that contact friction dominates over collisions.

The friction number N_{Fric} is used to compare the relative effects of particle contact friction and pore fluid viscous shearing (Iverson, 1997):

$$N_{Fric} = \frac{N_{Bag}}{N_{Sav}}. \quad (5)$$

This number expresses the ratio of the shear stresses caused by enduring grain contacts and pore fluid viscous shearing. Values for N_{Fric} calculated in our experiment were 6×10^5 for the first series and 5×10^4 for the second series. These large values (>100) suggest that the solid frictional shear stresses probably exceeded the pore fluid viscous shearing stresses (Zhou & Ng, 2010).

In conclusion, the dimensionless numbers above indicate that the flow in our experiments was laminar in a macro-viscous regime where the effects of the interstitial fluid were dominant and collisional interactions were negligible.

Segregation

The final deposits show clear particle segregation: smaller, denser red (representing chromite) particles were deposited at the base and were then overlain by white medium-sized particles (representing pyroxene), which were then in turn overlain by larger, lighter black particles (representing plagioclase) at the top (Figs 5 and 6). The segregation mechanism was fast and effective, but dependent on the inclination angle. Indeed, very early during the run-out, the segregation was even more obvious and well marked for experiments with a steep slope (Figs 5a and 6a).

In scrutinizing the flow during slumping via the video recordings (see Supplementary Data), we observe that the larger black particles gradually rose to the surface, whereas the smaller red beads percolated down to the bottom of the box. The white medium-sized particles were sandwiched between. This combination of percolation and squeeze-expulsion processes in dry conditions for an inclined downslope is visually similar to the mechanism of 'kinetic sieving' (Savage & Lun, 1988; Gray & Thornton, 2005; Gray & Chugunov, 2006). Our dimensional study, however, suggests that the effect of the viscous interstitial fluid is important during the flow in our experiments, which rules out kinetic sieving as the sole mechanism driving segregation. To our knowledge, none of the studies (e.g. Stix, 2001; Choux *et al.*, 2004; Hodson & Alexander, 2010; Mériaux & Kurz-Besson, 2012) that addressed particle segregation downslope in wet conditions (i.e. cases where the air is completely replaced by a liquid) have proposed a mechanical description of particle segregation. We thus simply characterize the systematic unmixing we observe as 'viscous particle segregation'. In none of our experiments was normal grading (i.e. larger particles at the base and smaller ones at the top of the flow) observed.

Anatomy of final deposits

During slumping, the flows were deposited continuously throughout the tank. A good example is experiment MB020, a time sequence of which is presented in Fig. 7. A front flow was created by opening the gate, with the material then rushing down the slope. On the whole, the final deposits were typically characterized by three regions that vary in size with the slope and the number of small beads, as shown in Fig. 8a: (1) the head or front flow, which contained the largest concentration of larger particles; (2) the body of the flow directly behind the front flow, which was thicker than the rest of the flow; finally, (3) the tail of the flow, in which particle concentration decreased significantly. Additionally, in some experiments, we observed an accumulation of larger particles at the head and on the periphery of the body of the flow, forming a more or less slight depression in the middle of the final deposits (Fig. 8b). These accumulations are known as 'levees'. This is a common feature in the case of mass flows such as avalanches, and grain and debris flows (Félix & Thomas, 2004; Lube *et al.*, 2007; Mangeney *et al.*, 2007).

A detailed study of the anatomy of the final deposits in this study is given below. Because of their low proportion, progression of the smaller beads located at the base of the flow was observed only in the experiments of the first series, with the mirror placed underneath the Perspex tank. Thus, first, we describe the anatomy of deposits with 0·5% of small red beads at different slopes and then we compare them with the deposits made by flows with 10% of small red beads.

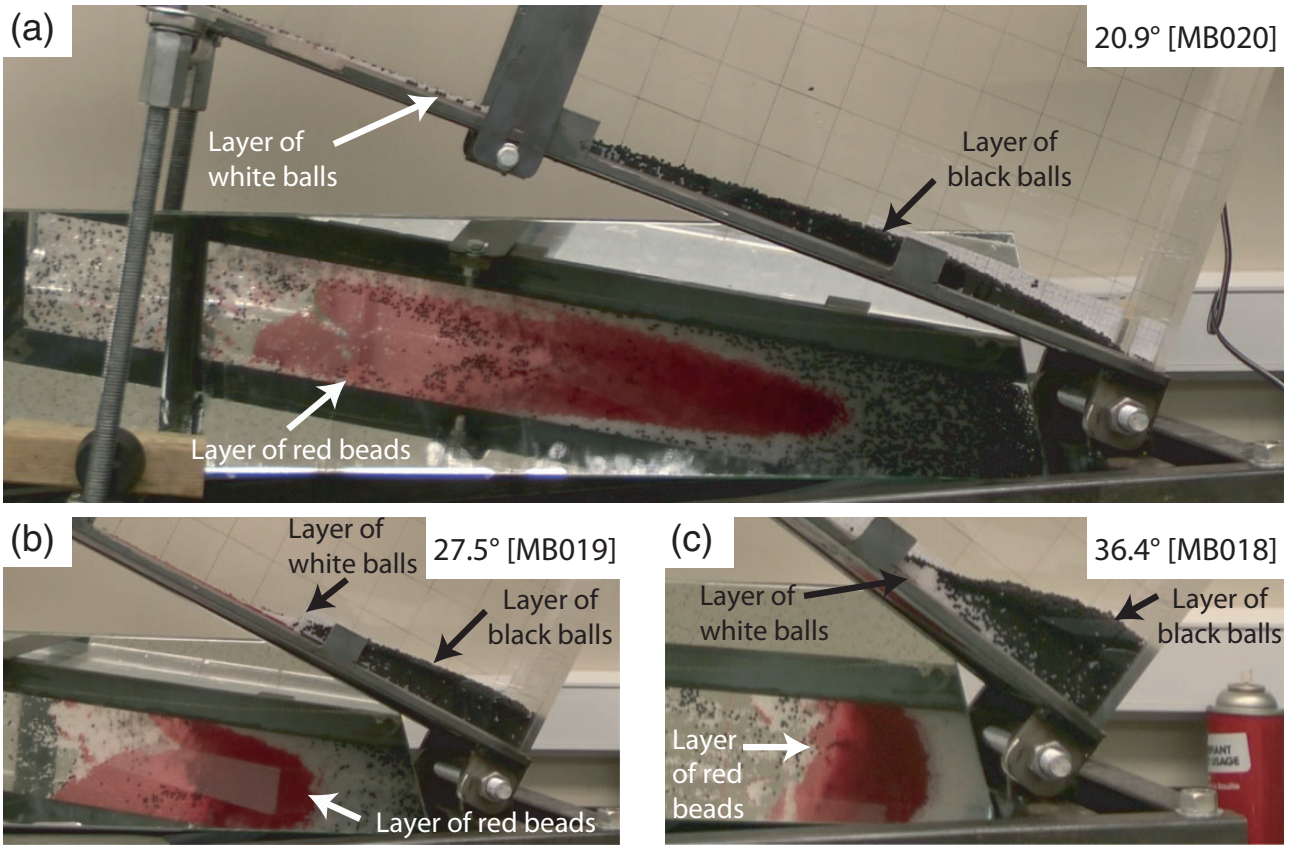

Fig. 5. Deposits obtained in the experimental series with 0·5 vol. % red glass beads. The general shape changes with inclination angle.

Series 1: 0·5% small beads

For small slopes ($15 < \alpha < 25°$), deposits covered most of the length of the tank. The tail of the deposit was very well developed and represented almost two-thirds of the final deposit length (Fig. 5a). The body was slightly thicker than the head and the tail, and thickened with increasing slope. Segregation was observed for the white and black particles. The small dense red beads were also separated and concentrated at the base of the flow. They exhibited a finger-like shape at the centre of the deposit, which is narrow and highly elongated (Fig. 5a). From the top view, the deposit body showed lateral 'levee' structures with a small central depression.

For intermediate inclinations ($25° < \alpha < 35°$), the head and body of the deposit could not be readily distinguished and the tail almost disappeared (Fig. 5b). The thickness of this accumulation was nearly uniform, but slightly thinner at the back. Segregation between white and black particles was observed in the tail of the deposit. From the top view, a depression was visible and was composed only of smaller beads surrounded by well-marked lateral levees and the deposit head. The red beads also showed a finger-like shape at the base, as was observed with small inclination angles, but it was shorter and wider.

At the high inclinations ($\alpha > 35°$), all the beads were concentrated at the end of the tank. The thickness of the deposit increased exponentially with distance from the gate. The top of the deposit did not show any depression or levees. Segregation between white and black balls was observed from the tail to the middle of the deposit, the front being well mixed owing to back flow against the end-wall. The distribution of the smaller beads at the flow base was the same as for intermediate inclination angles and showed a dome shape corresponding to the increase in the inclination angle (Fig. 5c).

Series 2: 10% small beads

At small inclination angles ($\alpha < 25°$), the deposit showed a widespread dispersion in the tank with an anatomy similar to the experiments with 0·5% small beads. The layering was well marked, with a regular and uniform thickness, except for the head of the flow where the larger beads were mixed and not well sorted owing to flow reflection at the end-wall. From the top, the rear central part of the deposit contained a depression composed only of small beads, surrounded by very small levees (Fig. 6a).

In experiments with intermediate inclination angles ($25° < \alpha < 35°$), the deposit occupied half the tank length and the thickness of the deposit increased linearly with the distance from the gate. Segregation was very well developed in most of the deposit, except for a region of

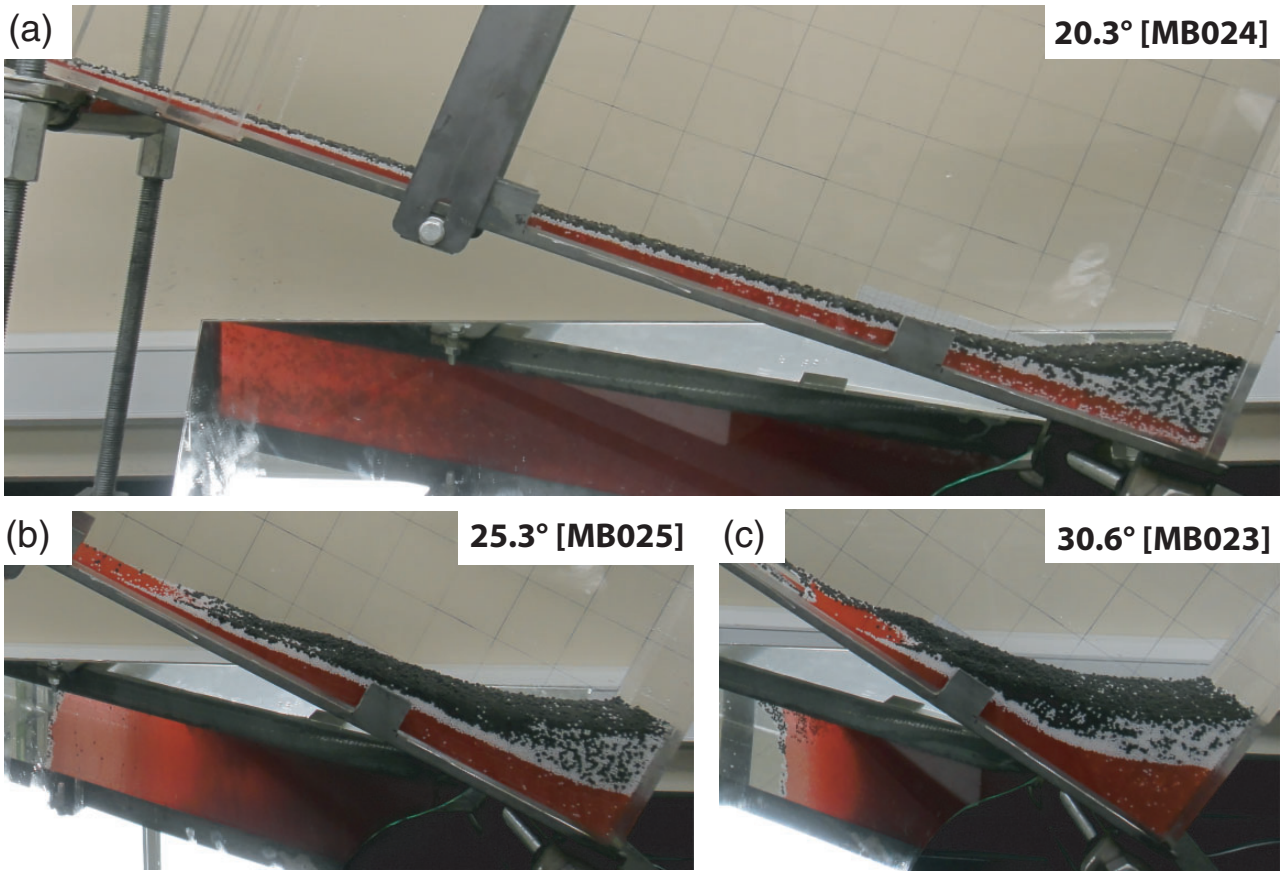

Fig. 6. Final deposits of the experiments with 10 vol. % red glass beads.

white and black beads at the end-wall. The red bead layer was not mixed with the other balls. On the top surface, levees and depressions were clearly observed. One-third of the deposit was composed solely of small beads with no covering (Fig. 6b and c).

Summary

During run-out flows deposited continuously throughout the tank and were well sorted, with the smallest beads at the base and the largest at the top. The final deposits were formed by piling up the beads, as observed in the video recordings (see Supplementary Data). The shape of the small-bead-dominated deposit varied with the inclination angle (Figs 5 and 6). For small angles (less than 25°), the deposit of red beads (representing chromite) had a finger-like shape, comprising a very elongated tail and a narrow head; its thickness was more or less uniform all along the deposit. Layering was visible in the tail of the final deposits. With an increase in the inclination angle, the shape became curved and shorter, more like a half disc: the tail disappeared and the body and head formed one longer continuous part. Layering was still visible, but the thickness of the layers was variable with the slope. Experiments with 10 vol. % of small red glass beads exhibited the same general progression in shape as a function of inclination angle. Layering was well marked in these experiments, especially for the glass beads, owing to their high proportion in the starting mixture. A front head region and levee formation were observed in the experiments (Fig. 8b), and were very well defined for the experiment with 10 vol. % of glass beads.

Multiple injection experiment

One additional experiment was carried out to investigate whether cyclic chromite layering could be reproduced after multiple slumping of the particles in the tank. The result was not what we expected. After segregation deposition of the first flow, the particles of the second flow were released. They also segregated by grain size and density during the flow, but each type of particle joined the layer formed by the same particles created by the previous flow, rather than piling up above the particles of the first flow. Hence, each monoparticle layer was thickened (Fig. 9). In the part close to the end-wall, the larger and intermediate particles were fairly well mixed. Once the second flow had reached the end-wall, particles of the third flow were released.

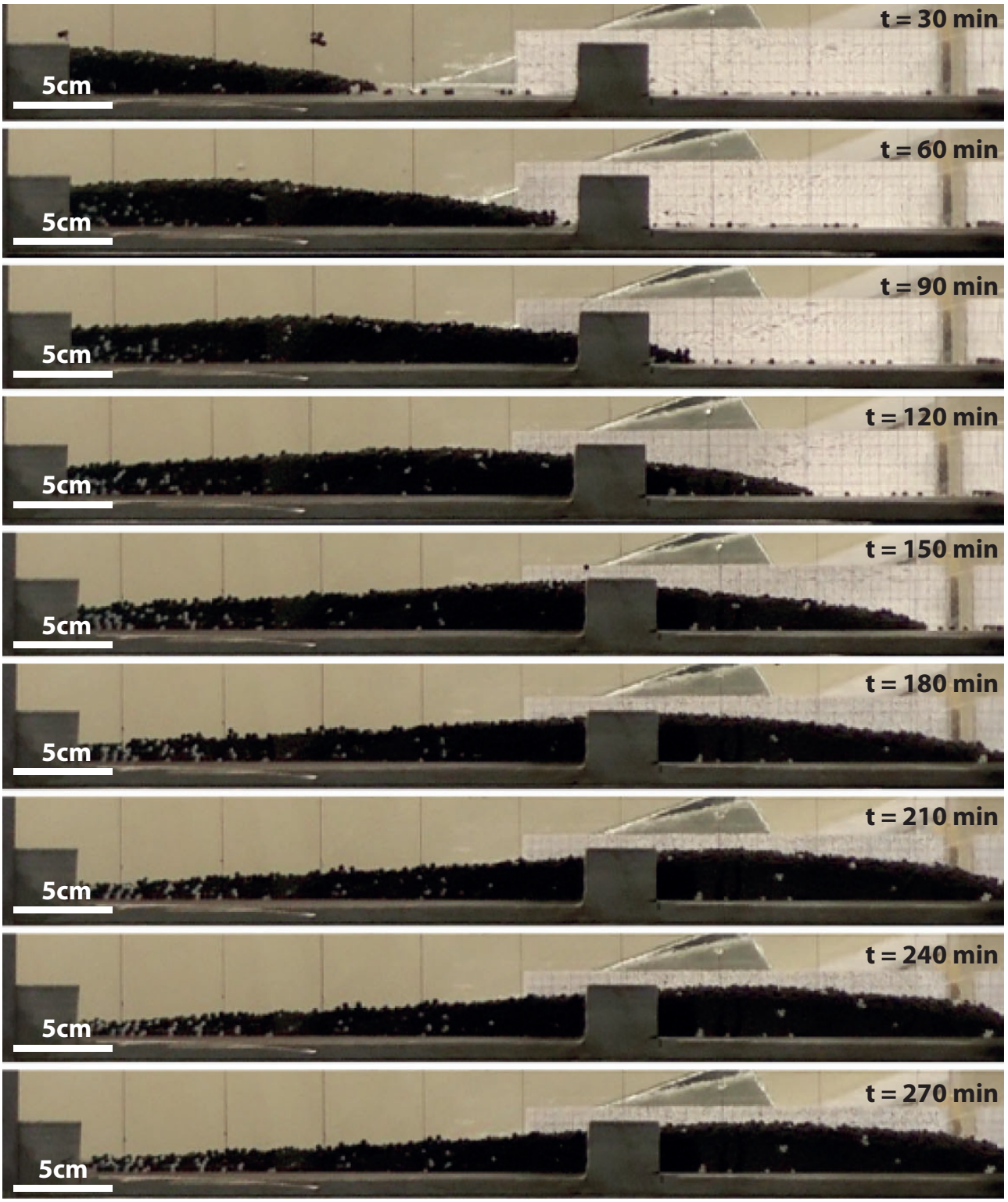

Fig. 7. Time sequence showing the side view of experiment MB020 during run-out.

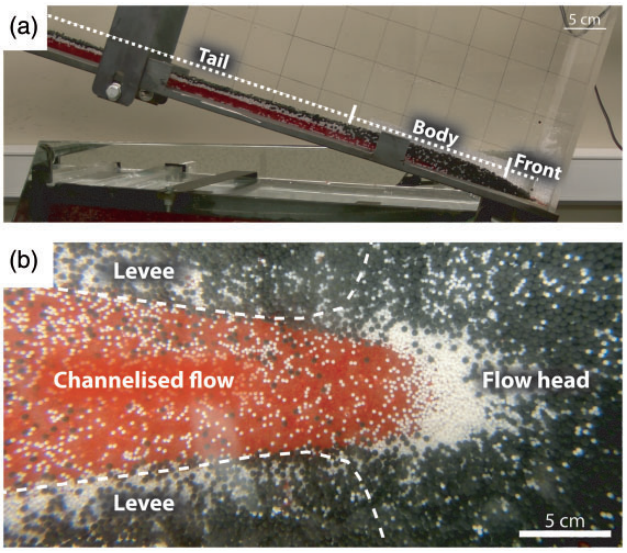

Fig. 8. (a) Anatomy of the flow showing three parts: the front or flow head, the body and the tail of the flow. (b) Overhead view of experiment MB027. The main features are the flow head and the channelized flow bounded by lateral levees that extend back along the flume.

The particles segregated, but the flow stopped ~34 cm from the end-wall, as shown in Fig. 9.

DISCUSSION

In this study we investigated the behaviour of a mixture of particles of different sizes and densities flowing down an inclined tank filled with a viscous fluid. Two series of experiments (one with 0·5% smaller particles, another with 10% smaller particles) at different inclinations (between 15° and 45°) were carried out. The results show a progression in particle migration and segregation during the flow; this produced layered deposits with thicknesses dependent on the inclination angle and on the proportion of small particles present.

Flow regime

Four dimensionless numbers were calculated and help us describe the relationship between inertial, gravitational, collisional, frictional and viscous forces during the flow [equations (1)–(4)]. The bulk flow dynamics is dominated by gravitational and viscous forces. With values of Bagnold numbers below the limit of 40 in our experiments, the dynamics of the suspension can be considered to be in a macro-viscous regime, which means that the effect of the viscosity of the interstitial fluid is relatively high. In this macro-viscous regime energy is dissipated by viscous interaction between particles and fluid. With values of the Savage number smaller than 0·1 and values of the friction number very large, contact friction dominates particle–particle dynamics.

Segregation

As shown in both experimental series, the segregation mechanism is effective, fast and always well developed in the tail of the flow. This is highlighted in the experimental series with 10 vol. % glass beads (Fig. 6). In our experiments, we observed via video recordings during the flow that the processes leading to segregation were a downward movement of smaller glass beads through voids that were present between larger particles, whereas the latter rose to the surface. This segregation mechanism is traditionally explained by (1) a void-filling mechanism whereby smaller particles percolate through the spaces between the larger particles and are thus found at the bottom of the flow (Savage & Lun, 1988) and (2) force imbalances driving a reverse flow of large particles towards the free surface by a process known as 'squeeze expulsion' (Thornton *et al.*, 2006). This process is called 'kinetic sieving' in granular flows in dry conditions (Middleton, 1970; Savage & Lun, 1988; Vallance, 1994; Gray & Thornton, 2005; Gray & Chugunov, 2006; Goujon *et al.*, 2007) or 'shear-induced segregation' in granular shear zones (German, 1989; Nedderman, 1992). However, our experiments were carried out in wet conditions and the dynamics of the flows are in a macro-viscous, laminar regime. Segregation processes occurring under such conditions are not well known, as most experimental studies (Stix, 2001; Choux *et al.*, 2004; Hodson & Alexander, 2010; Mériaux & Kurz-Besson, 2012) have been carried out in the turbulent regime. Another issue is that previous studies addressing the effect of the interstitial liquid involved fluids far less viscous than the glycerin used in our experiments (Vallance & Savage, 2000; Jain *et al.*, 2004; Chou *et al.*, 2011). Notwithstanding these dissimilarities, one universal observation is that the segregation mechanism is affected by the proportions of coarse and fine particles (Goujon, 2004; Roche *et al.*, 2005) and shapes (Makse *et al.*, 1997; Kleinhans, 2004, 2005).

Density and viscosity of interstitial fluid

As demonstrated above, the interstitial fluid plays a key role in the dynamics of the flow. Indeed, the interstitial fluid supplies a cohesive force between the grains, which is assumed to be negligible in dry conditions. The dynamics are those of gravity currents, which obey the normal laws of fluid mechanics and in which the grains are suspended by the vertical component of fluid velocity. In a viscous fluid, the particles do not rebound on each other following collisions because the kinetic force is absorbed by viscous drag (Jain *et al.*, 2004). Samadani & Kudrolli (2000) observed a sharp reduction in the segregation in granular flows when a small volume fraction of fluid was added. However, a transition back to segregation was observed when particles were completely immersed in fluid because, in this case, liquid bridges and capillary forces are absent, but viscous forces are present. Chou *et al.* (2014) showed that an increase in the fluid viscosity causes an increase in

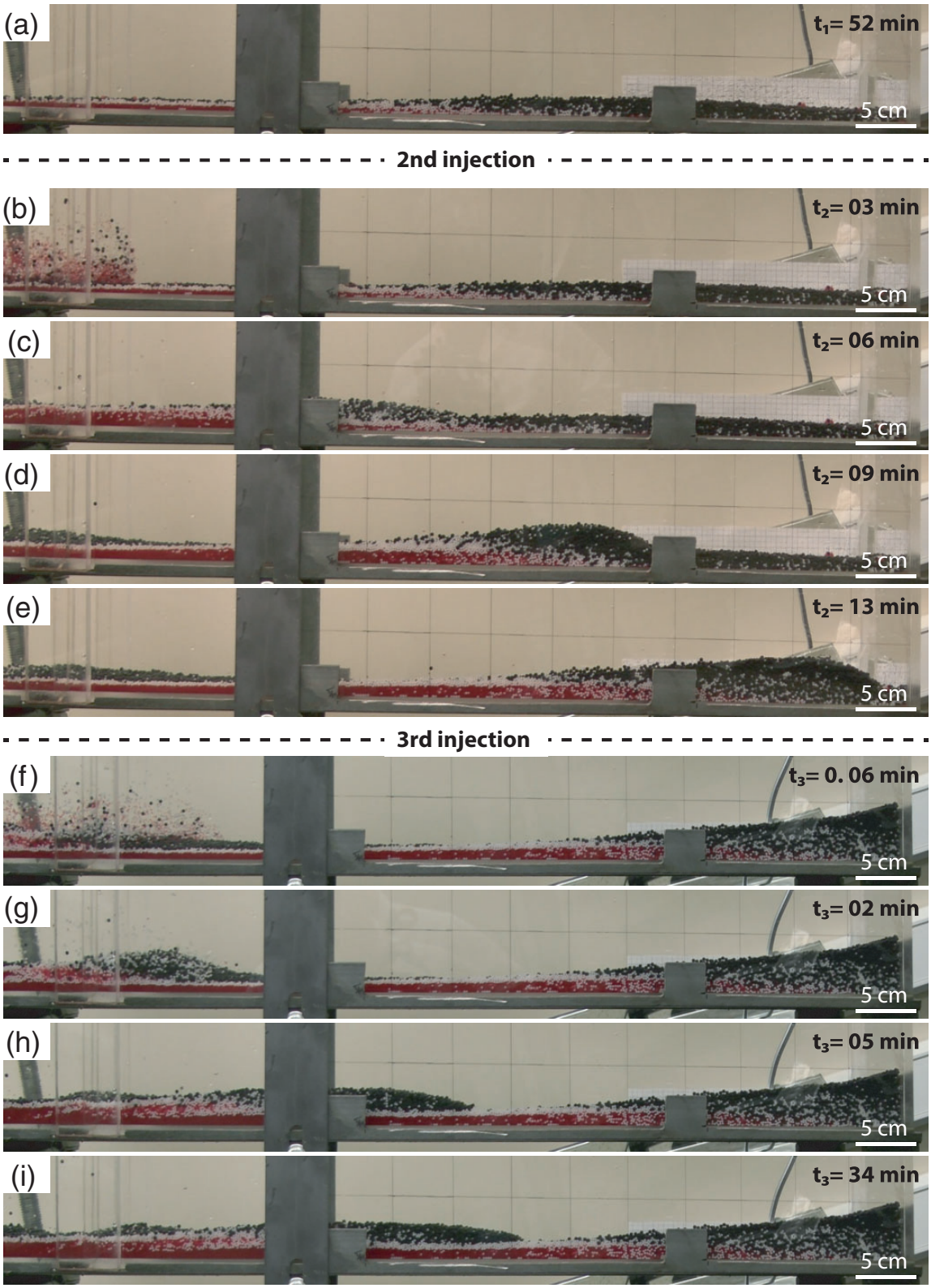

Fig. 9. Time sequence of the multi-injection experiment. (a) No movement was observed after 52 min from the first injection. The flow of the second injection (b–d) forms a second 'wave' and reaches the end of the flume (e). Finally (f, g) the flow third injection creates a new 'wave', which stops after 5 min (h, i).

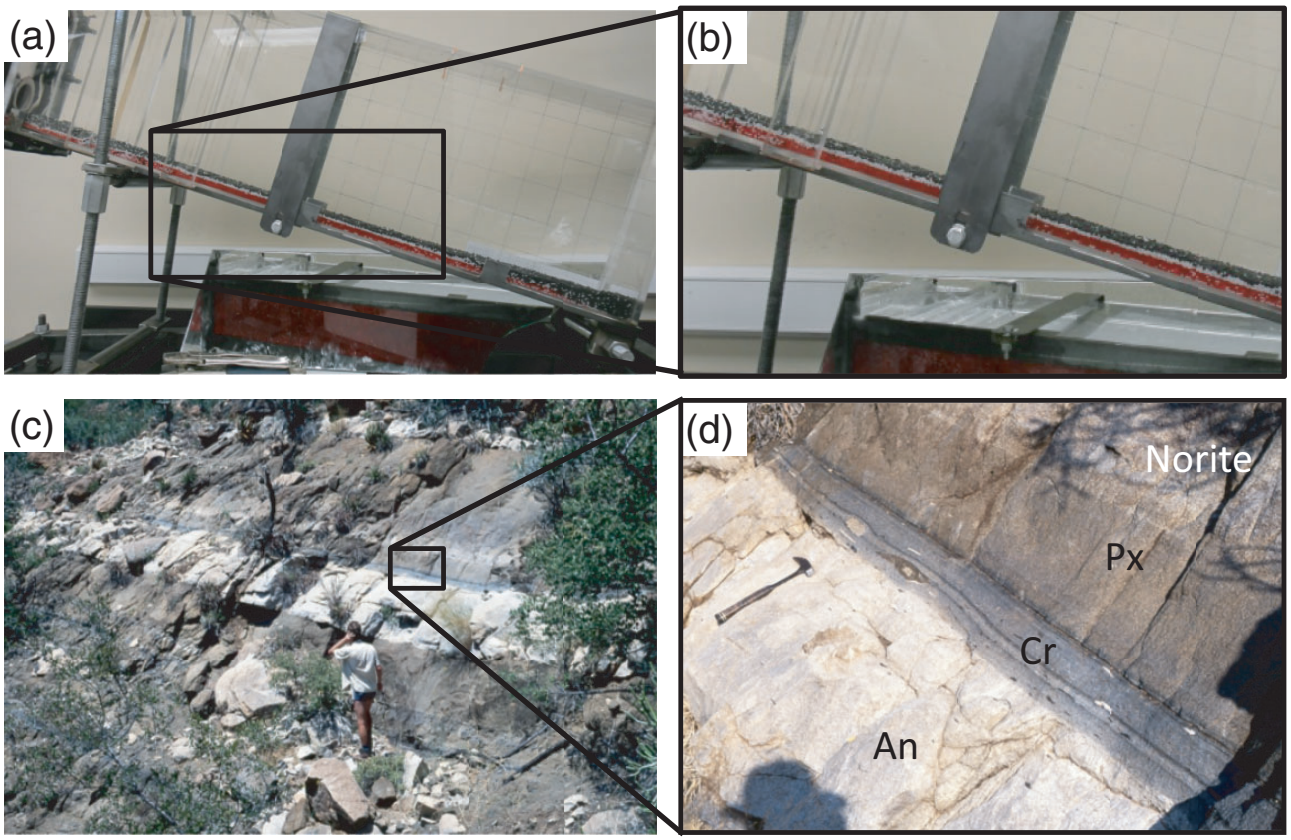

Fig. 10. Layering observed in analogue experiment MB026 (a, b) is compared with a natural example from Jagdlust, Eastern Bushveld Complex, South Africa (c, d) at the LCZ–UCZ boundary where an anorthosite has an overlying MG3 chromite seam. In the close-up (b), we can see that the sequence of layers from the bottom to the top is: red glass beads (representing chromitite), white polyacetal balls (representing pyroxenite) and black silicone balls (representing anorthosite). This sequence can be compared with the close-up (d) of the natural example where the sequence of the layers from bottom to top is: chromitite (Cr), pyroxenite (Px) and norite. The anorthosite (An) is located at the bottom of the sequence and represents the top of a previous sequence. Photographs (c) and (d) courtesy of D. Reid.

the angle of repose, and Thornton *et al.* (2006) and Vallance & Savage (2000) showed that it is not the viscosity of the fluid that influences the segregation process, but the density of the fluid. In their experiments, Vallance & Savage (2000) showed that the fluid density has a large effect on segregation, and a complete suppression of segregation is possible where the fluid and particle densities match. Moreover, Thornton *et al.* (2006) showed that the buoyancy induced by the interstitial fluid is more important than the effects of viscosity in the high solid fraction experiments of Vallance & Savage (2000).

Owing to the paucity of reported experiments in immersed conditions, we used the equivalent literature on experiments in dry conditions to better understand the viscous particle segregation mechanism occurring in our experiments. In dry conditions, this mechanism is called 'kinetic sieving' and it is mostly based on a sorting of particles by size and density contrast (Savage & Lun, 1988; Vallance, 1994). However, in geophysical mass flows, mechanisms other than kinetic sieving and squeeze expulsion may drive and modulate particle segregation, such as the dispersive pressure mechanism. Indeed, because dispersive pressure has a strong dependence on particle diameter, it has been speculated that it could affect particles of variable sizes differently. However, this explanation is not definitive, as it could also lead to the opposite conclusion that small particles rise to the top (Legros, 2002). Our experiments do not generate significant pore pressure (high N_{Fric}), but increasing fluid viscosity while keeping all other variables constant would increase dispersive pressure. In high-concentration parts of pyroclastic flows, large pumice fragments may segregate upwards because they are positively buoyant (*Sparks*, 1976; *Branney & Kokelaar*, 2002). However, segregation may be hindered by a wide distribution of grain sizes (*Gray & Ancey*, 2011).

Size ratio

The size ratio between the particles is the main factor in the efficiency of the segregation process in dry conditions (Rosato *et al.*, 1987). The experiments of Thomas

(2000) and Félix & Thomas (2004) showed that size segregation of particles of the same density is dominated by a dynamic sieving process at small size ratios (<5). However, at very large size ratios between the particles (>8), a mass effect (push-away process) is dominant and causes an 'inverse' segregation—larger particles are found at the base of the flow overlain by the smaller ones. In our experiments, the size ratio between the larger and the smaller beads (d_l/d_s) was approximately 4·3, which leads us to consider that size contrast played a role in the segregation process.

Particle density

Grains in gravity-driven flows can segregate by density contrast alone. A particularity in our experiments was that the smaller beads were also denser, whereas the larger particles were lighter. Hence, it is difficult to determine which of size or density drove the segregation in our experiments. In the case of 'kinetic sieving', it has been demonstrated that the size ratio is the main parameter for the segregation process. However, experimental work by Marsh (2013) also demonstrated that kinetic sieving can be enhanced by a higher density contrast between particle sizes to obtain better segregation or layering. Consequently, the segregation process in our study involves the additional effects of kinetic sieving and gravity dragging larger particles downwards.

Grain shape

Although the density ratio of the particles was scaled as closely as possible to that of natural minerals, one of the limitations in our experiments was the scaling of the grain shape. The materials used as analogues for crystals, although having a good agreement for the density ratio, were unfortunately similar in shape to each other (i.e. spheres), and differed in shape from the natural crystals they were used to represent. This simplification should not greatly affect the behaviour of chromite and olivine crystals, which generally have equant crystal shapes, but pyroxene and plagioclase are tabular to prismatic and this could have a major effect. Particles with tabular and elongated shapes have higher angles of repose (~90°, Stokely *et al.*, 2003) compared with spherical particles with lower angles of repose (32° for dry sand). This could influence the flow, the segregation processes and also the morphology of the final deposits. If the crystals all have the same shape, the aspect ratio is small and the internal coherence is low. The particles can be easily detached and flow independently (Farris, 1968). However, in a mixture of spherical and elongated crystals, particles with different aspect ratios are randomly oriented and, if they are in random close-packing conditions, have many points of contact with other particles. In these conditions, the particles could move as a coherent block and it is likely that such a block would 'bounce' or roll down the walls as opposed to flowing down them (Olson *et al.*, 2000). Furthermore, the flow of elongated particles can cause their alignment (McBirney & Nicolas, 1997; Ehrentraut & Chrzanowska, 2003; Cimarelli *et al.*, 2011) in the final deposits. Mineral alignment was observed by Mondal & Mathez (2007) in Upper Group 2 (UG2) of the Bushveld intrusion where elongated orthopyroxene and plagioclase crystals are aligned parallel to layering. Ehrentraut & Chrzanowska (2003) also demonstrated this effect using rice grains on a slope, showing that the grains aligned within the flow field for the case of a simple shear flow.

Basal rough plane

In all the experiments of our study, the particles flowed on a smooth plane, which is considered ideal, with minimal friction between the particles at the base of the flow and the plane. However, in natural systems, the basal plane would be irregular. Phillips *et al.* (2006) and Linares-Guerrero *et al.* (2007) have shown that particle segregation reduces basal friction, with small particles acting as rolling balls; thus, we consider that the smooth surface of our experiments is not a serious impediment to extrapolating the results to natural systems. Moreover, the absence of a rough basal plane allowed us to observe the shape of the small bead deposits. These deposits show a similar profile independent of the angle of inclination. They were concentrated at the centre of the flow and in lower concentrations on the sides (Fig. 5). This profile is similar to the so-called Couette profile developed in a channel, where the flow velocity is maximum at the flow centre and is slowed at the wall contacts by side-wall friction (GDR MiDi, 2004; Jop *et al.*, 2005). This is in agreement with the low Reynolds number calculated for these experiments.

Velocity

In the experiments with a low number of small beads, larger particles moved faster than the smaller ones (Fig. 4b). They were concentrated in the upper layers and were transported to the flow front, where they were carried to the side by the centre flow (made up of more mobile fine particles) and created static coarse-grained lateral levees that channelized the flow. These levees were also observed in the final deposits (Fig. 8b). Because the concentration of larger particles occurred at the flow front and at the margins, the smaller particles concentrated at the centre and in the tail, creating two zones during the flow. Iverson (1997) and Parsons *et al.* (2001) observed similar self-organization in their experiments and demonstrated that each zone has a distinctive rheological behaviour. In particular, the centre of the flow behaved more like a viscoplastic material, whereas the flow region close to the walls—where the levees were developed—was in a Coulomb frictional regime (having sustained solid frictional contact between grains). We also observed that the front flow velocity was faster with higher inclination angles and also that the morphology of the final deposits was

related to the inclination angle. With higher inclination angles, the final deposits were thicker but shorter. Although this result could be a consequence of the geometry of the experimental set-up, Félix & Thomas (2004) linked the frontal velocity of dry flows to the morphology of the final deposits, showing that the faster the front of the flow, the thicker and shorter are the final deposits for unconfined flows, as observed in our experiments.

Deposits

The final deposits in our experiments showed a layering of the particles segregated by particle type. Figures 5 and 6 show that the layering was well developed in the tails of the final deposits and had a homogeneous thickness along their length for inclination angles $<25^\circ$. For steeper slopes, the layering was more heterogeneous; the thickness of the layer of larger particles increased close to the end-wall, whereas it was the opposite for the smaller and intermediate size particles (i.e. the thickness of the layers of small particles decreased close to the end-wall). Indeed, during the flow, the first particles to reach the end-wall were the large ones and, because of their terminal velocity, they created a 'back flow' made up of black silicone balls. These balls were then in suspension just above the deposit, close, more or less, to the end-wall. When the balls settled they accumulated close to the end-wall, creating a layer of black silicone balls that was thicker close to the end-wall. At the same time, when the smaller and intermediate size particles reached the end-wall, no 'back flow' was created because of the larger particle cumulate already in place. The smaller and intermediate particles simply intruded into the base of the large particle cumulate. The resultant layer was hence thinner close to the end-wall and thicker towards the centre of the box.

Multi-injection experiment

A multi-injection experiment was carried out to observe the effects of repeated flows and whether cyclic layering could be created. Results were unexpected. After the first flow segregated, the second flow intruded into the first and each of the layers (smaller, intermediate and larger particle layers) thickened. The ease with which the second flow intruded into the first may be explained by a lack of consolidation of the first deposit. The layers in the first deposit were loose and easily intruded by particles of the second flow. The third flow stopped before reaching the end-wall. A possible explanation is that the third flow moved over an erodible floor created by the particles left by previous flows. This substrate was mobile and absorbed the kinetic energy of the third slump, reducing the particle terminal velocity and stopping the flow. Another possible explanation is that the third flow did not reach the end-wall because the deposits of the two previous flows lowered the bed slope too much. Indeed, despite the inclination angle of the box being the same for all three flows, the inclination angle of the floor formed by the accumulation of flows 1 and 2 was lower than the original angle of the tank. The slopes of the final deposits left after the first and second slumps were $16{\cdot}53^\circ$ and $11{\cdot}80^\circ$, respectively, and, as discussed above, we observed in our experiments that below 15° no flow occurred.

COMPARISON WITH NATURAL EXAMPLES

The experiments in our study can be extrapolated relatively well to layered intrusions, although they were conducted in a lock exchange apparatus. Our results can be applied to two problems of layered intrusion formation: the formation of layers from a homogeneous mixture of minerals and their geometry in fossil magma chambers.

We show that it is possible to form segregated layers from an initially homogeneous mixture of particles. The experimental results can be compared with natural examples. Figure 10 compares the final deposit of experiment MB026 with an example of layering found in the Bushveld Complex in South Africa. Both show similar stratification with (1) at the bottom, a layer of chromitite (corresponding in our experiments to the red glass beads layer), overlain by (2) a pyroxene cumulate layer (corresponding to the white polyacetal balls), followed by (3) a norite (corresponding to a mixture between the white polyacetal and black silicone balls) and finally (4) an anorthosite (corresponding to the black silicone balls) at the top.

The layering in our experiments can also be compared with the layering observed in the Great Dyke (Zimbabwe) or Stillwater Complex (Montana, USA). In these mafic to ultramafic intrusions the layering comprises an alternation of chromite, olivine and/or pyroxene monomineralic layers (Fig. 1c and d). In the case of the Stillwater Complex, layering in the A and B cycles consists of only dunite and chromitite layers (Cooper, 1997), with grain sizes varying from 1 to 1·5 mm for olivine grains and from 0·05 to 0·1 mm for chromite grains (Page, 1972). As in our experiments, the basal layer consists of smaller and denser minerals and the upper layer of larger and lighter minerals. Hence, it is conceivable that the layering observed in the Stillwater intrusion could be the result of particle segregation during the slumping of semi-consolidated cumulates.

Our results show that for experiments run with low inclination angles the final deposits are highly elongated and, hence, each layer is very thin and extensive, with a constant thickness. Examples of such extensive thin layers can be found in the Bushveld Complex as described by Lee (1996), the dips of which are 8–12°, or in the Muskox Intrusion (NW Canada), where the basement dips at 5–10° (Irvine & Smith, 1967). In contrast, for experiments with higher inclination angles, the deposits are concentrated over a short distance, so that the layers are both thicker and more variable in thickness; that is, thicker towards the middle and thinner at the walls of the tank. One natural example of a layered

intrusion showing such features is the Great Dyke (Zimbabwe), where layering is thicker towards the centre of the magma chamber and thinner at the walls, as described by Wilson & Prendergast (1989). The average dips of the layering range from 15° to 30° (Wilson & Prendergast, 2001). A similar observation can be made at the Duluth Complex (Minnesota, USA), where the layered series comprises a sequence of sheets dipping at 15–25° (Grout, 1949; Grout *et al.*, 1959) that thicken to the west.

Junge *et al.* (2014) showed that several sub-layers can be observed in a thick massive chromitite seam (UG2) in the Bushveld Complex. This observation can be compared with the final deposits of our multiple injection experiment where we observed that, when the slope stayed above the critical angle of repose, a new slumping of particles intruded previous deposits and each layer was thickened. Each new slumping could be the source of a new sub-layer, as observed by Junge *et al.* (2014) for the Bushveld Complex.

The low viscosity of the experimental fluid, which matches that of the mafic magma that formed the Bushveld Complex, unfortunately does not allow the extrapolation of the observed segregation to higher melt viscosities. Higher viscosities would cause pore pressure to dominate over frictional forces, which would affect segregation efficiency. It has recently been suggested that the low Reynolds number prevailing in most magmatic systems (Glazner, 2014) inhibits physical rearranging of crystals. Our results show that crystal-laden flows in the laminar regime are multiple and complex. This rich dynamics includes efficient segregation and cannot be understood solely in the light of the Reynolds number.

CONCLUSIONS

The main aim of this study was to investigate whether slumping of semi-consolidated cumulates could be the source of mineral layering in the Bushveld Complex. In this model, the semi-consolidate cumulates are homogeneous mixtures of different mineral species (chromite, pyroxene and plagioclase) formed by crystallization in cotectic proportions on the side-wall of the magma chamber. In our experiments, similar conditions were reproduced with a mixture of different beads (representing mineral species), replicating cotectic proportions, and glycerine (mimicking the magma). This starting material was introduced, in an inclinable flume tank, in such a manner as to obtain a homogeneous mixture of beads at the start of the experiment. The final deposits, formed after the run-out of the beads, showed that it is possible to achieve layering via a process involving viscous segregation in which the smaller, denser particles percolate down though spaces between the larger, less dense grains in a viscous fluid. Our results show that the dynamics of the flow are in a macro-viscous regime in which the frictional grain contacts dominate. We demonstrate that the final deposits are elongated and thin, with a uniform thickness after slumping at a low angle of inclination, as observed for natural systems such as the Bushveld Complex in South Africa. In contrast, our experiments show that after slumping down a steeper slope the final deposits occupy a small area, but are thicker with a heterogeneous thickness—thicker towards the flow head and thinner towards the flow tail—which is observed in layered intrusions with steeply inclined walls such as the Great Dyke (Zimbabwe) or Kemi intrusion (Finland). The multi-injection experiment allowed us to observe that it is possible to thicken previous layers, if they are not consolidated, by injection.

Our results show that the physical process of particle segregation in a viscous fluid can account for mineral layering in layered intrusions. Moreover, our experiments show that the thickness and distribution of the layers is related to the slope of the magma chamber walls.

ACKNOWLEDGEMENTS

We thank Mr. P. Vandal from C.U.R.A.L. for building our Perspex flume tank, and Mr D. Noel and Mme M. Doucet for making laboratory space available and for their advice. We thank Vernon Manville, Bruce Marsh, two anonymous reviewers and the editor, Marjorie Wilson, for their helpful reviews of this paper.

FUNDING

This work was funded by the Canada Research Chair Magmatic Ore Deposits (grant #950-215503).

SUPPLEMENTARY DATA

Supplementary data for this paper are available at *Journal of Petrology* online.

REFERENCES

Allen, J. R. L. (1970). The avalanching of granular solids on dune and similar slopes. *Journal of Geology* **78**, 326–351.

Balmforth, N. J., Craster, R. V., Perona, P., Rust, A. C. & Sassi, R. (2007). Viscoplastic dam breaks and the Bostwick consistometer. *Journal of Non-Newtonian Fluid Mechanics* **142**, 63–78.

Barenblatt, G. I. (2003). *Scaling*. Cambridge University Press.

Barnes, S.-J., Maier, W. D. & Curl, E. A. (2010). Composition of the marginal rocks and sills of the Rustenburg Layered Suite, Bushveld Complex, South Africa: implications for the formation of the platinum-group element deposits. *Economic Geology* **105**, 1491–1511.

Blanchette, F., Peacock, T. & Bush, J. W. M. (2004). The Boycott effect in magma chambers. *Geophysical Research Letters* **31**, doi:10.1029/2003GL019235.

Bonnecaze, R. T., Huppert, H. E. & Lister, J. R. (1993). Particle-driven gravity currents. *Journal of Fluid Mechanics* **250**, 339–369.

Branney, M. J. & Kokelaar, B. P. (2002). *Pyroclastic Density Currents and the Sedimentation of Ignimbrites. Geological Society, London, Memoirs* **27**, 152 pp.

Bursik, M., Patra, A., Pitman, E. B., Nichita, C., Macias, J. L., Saucedo, R. & Girina, O. (2005). Advances in studies of

dense volcanic granular flows. *Reports on Progress in Physics* **68**, 271–301.
Cameron, E. N. (1975). Postcumulus and subsolidus equilibration of chromite and coexisting silicates in the Eastern Bushveld Complex. *Geochimica et Cosmochimica Acta* **39**, 1021–1033.
Cameron, E. N. (1980). Evolution of the Lower Critical Zone, central sector, eastern Bushveld Complex, and its chromite deposits. *Economic Geology* **75**, 845–871.
Cameron, E. N. & Desborough, G. A. (1964). Origin of certain magnetite-bearing pegmatites in the eastern part of the Bushveld complex, South Africa. *Economic Geology* **59**, 197–225.
Carrigy, M. A. (1970). Experiments on the angles of repose of granular materials. *Sedimentology* **14**, 147–158.
Castruccio, A., Rust, A. C. & Sparks, R. S. J. (2010). Rheology and flow of crystal-bearing lavas: Insights from analogue gravity currents. *Earth and Planetary Science Letters* **297**, 471–480.
Cawthorn, R. G. (2005). Pressure fluctuations and the formation of the PGE-rich Merensky and chromitite reefs, Bushveld Complex. *Mineralium Deposita* **40**, 231–235.
Chou, H. T., Chou, S. H. & Hsiau, S. S. (2014). The effects of particle density and interstitial fluid viscosity on the dynamic properties of granular slurries in a rotating drum. *Powder Technology* **252**, 42–50.
Chou, S. H., Liao, C. C. & Hsiau, S. S. (2011). The effect of interstitial fluid viscosity on particle segregation in a slurry rotating drum. *Physics of Fluids (1994–present)* **23**, 083301.
Choux, C., Druitt, T. & Thomas, N. (2004). Stratification and particle segregation in flowing polydisperse suspensions, with applications to the transport and sedimentation of pyroclastic density currents. *Journal of Volcanology and Geothermal Research* **138**, 223–241.
Choux, C. M. & Druitt, T. H. (2002). Analogue study of particle segregation in pyroclastic density currents, with implications for the emplacement mechanisms of large ignimbrites. *Sedimentology* **49**, 907–928.
Cimarelli, C., Costa, A., Mueller, S. & Mader, H. M. (2011). Rheology of magmas with bimodal crystal size and shape distributions: Insights from analog experiments. *Geochemistry, Geophysics, Geosystems* **12**, Q07024.
Cimarelli, C., Costa, A., Mueller, S. & Mader, H. M. (2011). Rheology of magmas with bimodal crystal size and shape distributions: Insights from analog experiments. *Geochemistry, Geophysics, Geosystems* **12**, Q07024.
Cooper, R. W. (1997). Magmatic unconformities and stratigraphic relations in the Peridotite zone, Stillwater Complex, Montana. *Canadian Journal of Earth Sciences* **34**, 407–425.
Courrech du Pont, S., Gondret, P., Perrin, B. & Rabaud, M. (2003). Granular avalanches in fluids. *Physical Review Letters* **90**, 044301.
Eales, H. (1987). Upper Critical Zone chromitite layers at RPM Union section mine, western Bushveld complex. In: Stowe, C. W. (ed.) *Evolution of Chromium Ore Fields*. Van Nostrand Reinhold, pp. 144–168.
Eales, H. V. (2000). Implications of the chromium budget of the Western Limb of the Bushveld Complex. *South African Journal of Geology* **103**, 141–150.
Ehrentraut, H. & Chrzanowska, A. (2003). Induced anisotropy in rapid flows of nonspherical granular materials. In: Hutter, P. D. K. & Kirchner, D. N. (eds) *Dynamic Response of Granular and Porous Materials under Large and Catastrophic Deformations*. Springer, pp. 343–364.
Farin, M., Mangeney, A. & Roche, O. (2014). Fundamental changes of granular flow dynamics, deposition, and erosion processes at high slope angles: Insights from laboratory experiments. *Journal of Geophysical Research: Earth Surface* **119**, 504–532.
Farris, R. J. (1968). Prediction of the viscosity of multimodal suspensions from unimodal viscosity data. *Journal of Rheology* **12**, 281–301.
Félix, G. & Thomas, N. (2004). Evidence of two effects in the size segregation process in dry granular media. *Physical Review E* **70**, 051307.
GDR MiDi (2004). On dense granular flows. *European Physical Journal E* **14**, 341–365.
German, R. M. (1989). *Particle Packing Characteristics*. Metal Powder Industries Federation.
Glazner, A. F. (2014). Magmatic life at low Reynolds number. *Geology* **42**, 935–938.
Goujon, C. (2004). Ecoulements granulaires bidisperses sur plans inclinés rugueux. *Doctoral dissertation*. Université de Provence–Aix-Marseille I.
Goujon, C., Dalloz-Dubrujeaud, B. & Thomas, N. (2007). Bidisperse granular avalanches on inclined planes: A rich variety of behaviors. *European Physical Journal E* **23**, 199–215.
Gray, J. M. N. T. & Ancey, C. (2011). Multi-component particle-size segregation in shallow granular avalanches. *Journal of Fluid Mechanics* **678**, 535–588.
Gray, J. M. N. T. & Chugunov, V. A. (2006). Particle-size segregation and diffusive remixing in shallow granular avalanches. *Journal of Fluid Mechanics* **569**, 365–398.
Gray, J. M. N. T. & Thornton, A. R. (2005). A theory for particle size segregation in shallow granular free-surface flows. *Proceedings of the Royal Society of London, Series A* **461**, 1447–1473.
Grout, F. F. (1949). *The titaniferous magnetites of Minnesota*. Office of the Commissioner of the Iron Range Resources and Rehabilitation.
Grout, F. F., Sharp, R. P. & Schwartz, G. M. (1959). *The Geology of Cook County, Minnesota. Minnesota Geological Survey Bulletin* **39**.
Hodson, M. E. (1998). The origin of igneous layering in the Nunarssuit syenite, South Greenland. *Mineralogical Magazine* **62**, 9–27.
Hodson, J. M. & Alexander, J. (2010). The effects of grain-density variation on turbidity currents and some implications for the deposition of carbonate turbidite. *Journal of Sedimentary Research* **80**, 515–528.
Hubbert, M. K. (1937). Theory of scale models as applied to the study of geologic structures. *Geological Society of America Bulletin* **48**, 1459–1520.
Huppert, H. E. (1982). Flow and instability of a viscous current down a slope. *Nature* **300**, 427–429.
Huppert, H. E. (2006). Gravity currents: a personal perspective. *Journal of Fluid Mechanics* **554**, 299–322.
Huppert, H. E. & Sparks, R. S. J. (1984). Double-diffusive convection due to crystallization in magmas. *Annual Review of Earth and Planetary Sciences* **12**, 11–37.
Hutter, K. (1984). Fundamental equations and approximations. In: Hutter, K. (ed.) *Hydrodynamics of Lakes*. Springer, pp. 1–37.
Irvine, T. N. (1975). Crystallization sequences in the Muskox intrusion and other layered intrusions—II. Origin of chromitite layers and similar deposits of other magmatic ores. *Geochimica et Cosmochimica Acta* **39**, 991–1020.
Irvine, T. N. (1977). Origin of chromitite layers in the Muskox intrusion and other stratiform intrusions: a new interpretation. *Geology* **5**, 273–277.
Irvine, T. N. (1982). Terminology for layered intrusions. *Journal of Petrology* **23**, 127–162.

Irvine, T. & Smith, C. (1967). The ultramafic rocks of the Muskox intrusion, Northwest Territories, Canada. In: Wyllie, P. J. (ed.) *Ultramafic and Related Rocks*. John Wiley, pp. 38–49.

Iverson, R. M. (1997). The physics of debris flows. *Reviews of Geophysics* **35**, 245–296.

Iverson, R. M. & Vallance, J. W. (2001). New views of granular mass flows. *Geology* **29**(2), 115–118.

Jain, N., Ottino, J. M. & Lueptow, R. M. (2004). Effect of interstitial fluid on a granular flowing layer. *Journal of Fluid Mechanics* **508**, 23–44.

Jop, P., Forterre, Y. & Pouliquen, O. (2005). Crucial role of sidewalls in granular surface flows: consequences for the rheology. *Journal of Fluid Mechanics* **541**, 167–192.

Junge, M., Oberthür, T. & Melcher, F. (2014). Cryptic variation of chromite chemistry, platinum group element and platinum group mineral distribution in the UG-2 chromitite: an example from the Karee Mine, Western Bushveld Complex, South Africa. *Economic Geology* **109**, 795–810.

Kinnaird, J. A., Kruger, F. J., Nex, P. A. M. & Cawthorn, R. G. (2002). Chromitite formation—a key to understanding processes of platinum enrichment. *Applied Earth Science: Transactions of the Institutions of Mining and Metallurgy: Section B* **111**, 23–35.

Kleinhans, M. G. (2004). Sorting in grain flows at the lee side of dunes. *Earth-Science Reviews* **65**, 75–102.

Kleinhans, M. G. (2005). Grain-size sorting in grainflows at the lee side of deltas. *Sedimentology* **52**, 291–311.

Kottke-Levin, J., Tredoux, M. & Gräbe, P.-J. (2009). An investigation of the geochemistry of the Middle Group of the eastern Bushveld complex, South Africa Part 1–the chromitite layers. *Applied Earth Science: Transactions of the Institutions of Mining and Metallurgy: Section B* **118**, 111–130.

Lee, C. A. (1996). A review of mineralization in the Bushveld Complex and some other layered intrusions. *Developments in Petrology* **15**, 103–145.

Legros, F. (2002). Can dispersive pressure cause inverse grading in grain flows? *Journal of Sedimentary Research* **72**(1), 166–170.

Linares-Guerrero, E., Goujon, C. & Zenit, R. (2007). Increased mobility of bidisperse granular avalanches. *Journal of Fluid Mechanics* **593**, 475–504.

Lipin, B. R. (1993). Pressure increases, the formation of chromite seams, and the development of the ultramafic series in the Stillwater Complex, Montana. *Journal of Petrology* **34**, 955–976.

Lube, G., Cronin, S. J., Platz, T., Freundt, A., Procter, J. N., Henderson, C. & Sheridan, M. F. (2007). Flow and deposition of pyroclastic granular flows: A type example from the 1975 Ngauruhoe eruption, New Zealand. *Journal of Volcanology and Geothermal Research* **161**, 165–186.

Maier, W. D., Barnes, S.-J. & Groves, D. I. (2013). The Bushveld Complex, South Africa: formation of platinum–palladium, chrome- and vanadium-rich layers via hydrodynamic sorting of a mobilized cumulate slurry in a large, relatively slowly cooling, subsiding magma chamber. *Mineralium Deposita* **48**, 1–56.

Makse, H. A., Cizeau, P. & Stanley, H. E. (1997). Possible stratification mechanism in granular mixtures. *Physical Review Letters* **78**, 3298.

Mangeney, A., Bouchut, F., Thomas, N., Vilotte, J. P. & Bristeau, M. O. (2007). Numerical modelling of self-channeling granular flows and of their levee-channel deposits. *Journal of Geophysical Research: Earth Surface* **112**, F02017.

Marsh, B. D. (2007). Magmatism, magma, and magma chambers. In: Watt, A. B. (ed.) *Treatise on Geophysics*. Elsevier, pp. 276–333.

Marsh, B. D. (2013). On some fundamentals of igneous petrology. *Contributions to Mineralogy and Petrology* **166**, 665–690.

McBirney, A. R. & Nicolas, A. (1997). The Skaergaard layered series. Part II. Magmatic flow and dynamic layering. *Journal of Petrology* **38**, 569–580.

McBirney, A. R. & Noyes, R. M. (1979). Crystallization and layering of the Skaergaard intrusion. *Journal of Petrology* **20**, 487–554.

McMillan, K., Long, P. E. & Cross, R. W. (1989). Vesiculation in Columbia River basalts. In: Reidel, S. P. & Hooper, P. R. (eds), Volcanism and Tectonism in the Columbia River Flood-basalt Province. *Geological Society of America, Special Papers* **239**, 157–168.

Mériaux, C. & Kurz-Besson, C. (2012). Sedimentation from binary suspensions in a turbulent gravity current along a V-shaped valley. *Journal of Fluid Mechanics* **712**, 624–645.

Middleton, G. V. (1970). Experimental studies related to problems of flysch sedimentation. In: Lajoie, J. (ed.), *Flysch Sedimentology in North America*. Geological Society of Canada, Special paper **7**, 253–272.

Mondal, S. K. & Mathez, E. A. (2007). Origin of the UG2 chromitite layer, Bushveld Complex. *Journal of Petrology* **48**, 495–510.

Murck, B. W. & Campbell, I. H. (1986). The effects of temperature, oxygen fugacity and melt composition on the behaviour of chromium in basic and ultrabasic melts. *Geochimica et Cosmochimica Acta* **50**, 1871–1887.

Naldrett, A. J., Kinnaird, J., Wilson, A., Yudovskaya, M., McQuade, S., Chunnett, G. & Stanley, C. (2009). Chromite composition and PGE content of Bushveld chromitites: Part 1—the Lower and Middle Groups. *Applied Earth Science: Transactions of the Institutions of Mining and Metallurgy: Section B* **118**, 131–161.

Naldrett, A. J., Wilson, A., Kinnaird, J., Yudovskaya, M. & Chunnett, G. (2012). The origin of chromitites and related PGE mineralization in the Bushveld Complex: new mineralogical and petrological constraints. *Mineralium Deposita* **47**, 209–232.

Naslund, H. R. & McBirney, A. R. (1996). Mechanisms of formation of igneous layering. In: Cawthorn, R. G. (ed.), *Layered Intrusions*, pp. 1–43.

Nedderman, R. M. (1992). *Statics and Kinematics of Granular Materials*. Cambridge University Press.

Nex, P. A. M. (2004). Formation of bifurcating chromitite layers of the UG1 in the Bushveld Igneous Complex, an analogy with sand volcanoes. *Journal of the Geological Society, London* **161**, 903–909.

Olson, C. J., Reichhardt, C., McCloskey, M. & Zieve, R. J. (2000). Effect of grain geometry on angle of repose and dynamics. *Europhysics Letters* **57**. doi: 10.1209/epl/i2002-00596-9.

Page, N. J. (1972). Grain-size variations within an olivine cumulate, Stillwater Complex, Montana. *US Geological Survey, Professional Papers* 800-**C**, 29–37.

Parsons, J. D., Whipple, K. X. & Simoni, A. (2001). Experimental study of the grain-flow, fluid–mud transition in debris flows. *Journal of Geology* **109**, 427–447.

Phillips, J. C., Hogg, A. J., Kerswell, R. R. & Thomas, N. H. (2006). Enhanced mobility of granular mixtures of fine and coarse particles. *Earth and Planetary Science Letters* **246**, 466–480.

Ramberg, H. (1981). *Gravity, Deformation, and the Earth's Crust: in Theory, Experiments, and Geological Application*. Academic Press.

Roche, O., Gilbertson, M. A., Phillips, J. C. & Sparks, R. S. J. (2005). Inviscid behaviour of fines-rich pyroclastic flows inferred from experiments on gas–particle mixtures. *Earth and Planetary Science Letters* **240**, 401–414.

Roche, O., Montserrat, S., Niño, Y. & Tamburrino, A. (2008). Experimental observations of water-like behavior of initially fluidized, dam break granular flows and their relevance for the propagation of ash-rich pyroclastic flows. *Journal of Geophysical Research: Solid Earth* **113**, 2156–2202.

Rosato, A., Strandburg, K. J., Prinz, F. & Swendsen, R. H. (1987). Why the Brazil nuts are on top: Size segregation of particulate matter by shaking. *Physical Review Letters* **58**(10), 1038.

Samadani, A. & Kudrolli, A. (2000). Segregation transitions in wet granular matter. *Physical Review Letters* **85**(24), 5102.

Savage, S. B. & Hutter, K. (1989). The motion of a finite mass of granular material down a rough incline. *Journal of Fluid Mechanics* **199**, 177–215.

Savage, S. B. & Lun, C. K. K. (1988). Particle size segregation in inclined chute flow of dry cohesionless granular solids. *Journal of Fluid Mechanics* **189**, 311–335.

Shaw, H. R. (1972). Viscosities of magmatic silicate liquids; an empirical method of prediction. *American Journal of Science* **272**, 870–893.

Simpson, J. E. (1999). *Gravity Currents: In the Environment and the Laboratory*. Cambridge University Press.

Sparks, R. S. J. (1976). Grain size variations in ignimbrites and implications for the transport of pyroclastic flows. *Sedimentology* **23**, 147–188.

Sparks, R. S., Huppert, H. E., Koyaguchi, T. & Hallworth, M. A. (1993). Origin of modal and rhythmic igneous layering by sedimentation in a convecting magma chamber. *Nature* **361**, 246–249.

Stix, J. (2001). Flow evolution of experimental gravity currents: Implications for pyroclastic flows at volcanoes. *Journal of Geology* **109**, 381–398.

Stokely, K., Diacou, A. & Franklin, S. V. (2003). Two-dimensional packing in prolate granular materials. *Physical Review E* **67**, 051302.

Thomas, N. (2000). Reverse and intermediate segregation of large beads in dry granular media. *Physical Review E* **62**, 961.

Thornton, A. R., Gray, J. M. N. T. & Hogg, A. J. (2006). A three-phase mixture theory for particle size segregation in shallow granular free-surface flows. *Journal of Fluid Mechanics* **550**, 1–26.

Ulmer, G. C. (1969). Experimental investigations in chromite spinels. In: Wilson, H. D. B. (ed.) *Magmatic Ore Deposits*. Economic Geology, Monograph **4**, 114–131.

Vallance, J. W. (1994). Experimental and field studies related to the behavior of granular mass flows and the characteristics of their deposits. PhD thesis, Michigan Technological University, Houghton.

Vallance, J. W. & Savage, S. B. (2000). Particle segregation in granular flows down chutes. In: Rosato, A. D. & Blackmore, D. L. (eds), *IUTAM Symposium on Segregation in Granular Flows* **81**, 31–51.

Voordouw, R., Gutzmer, J. & Beukes, N. J. (2009). Intrusive origin for upper group (UG1, UG2) stratiform chromitite seams in the Dwars River area, Bushveld Complex, South Africa. *Mineralogy and Petrology* **97**, 75–94.

Wilson, A. H. & Prendergast, M. D. (1989). The Great Dyke of Zimbabwe—I: tectonic setting, stratigraphy, petrology, structure, emplacement and crystallisation. In: Prendergast, M. D. & Jones, M. J. (eds) *Magmatic Sulphides, the Zimbabwe Volume*. Institution of Mining and Metallurgy, 1–20.

Wilson, A. H. & Prendergast, M. D. (2001). Platinum-group element mineralisation in the Great Dyke, Zimbabwe, and its relationship to magma evolution and magma chamber structure. *South African Journal of Geology* **104**, 319–342.

Wilson, J. R., Menuge, J. F., Pedersen, S. & Engell-Sørensen, O. (1987). The southern part of the Fongen–Hyllingen layered mafic complex, Norway: emplacement and crystallization of compositionally stratified magma. In: Parsons, L. (ed.), *Origins of Igneous Layering*. Springer, pp. 145–184.

Zhou, G. G. & Ng, C. W. (2010). Dimensional analysis of natural debris flows. *Canadian Geotechnical Journal* **47**, 719–729.